lubricants

MDPI

Article

Prediction of Iron Wear Metal Concentration in Used Engine Oils from FT-IR Spectra Using Partial Least Squares Regression

Adam Agocs *, Georg Vorlaufer, Marcella Frauscher and Charlotte Besser

AC2T Research GmbH, 2700 Viktor Kaplan-Straße 2/C, 2700 Wiener Neustadt, Austria
* Correspondence: adam.agocs@ac2t.at

Abstract

Wear metal monitoring is an important component of lubricant condition monitoring but commonly relies on elemental techniques such as inductively coupled plasma optical emission spectroscopy (ICP-OES), which require dedicated laboratory infrastructure and sample preparation. This study evaluates whether Fourier-transform infrared (FT-IR) spectra of used engine oils can be combined with partial least squares (PLS) regression to provide a rapid screening estimate of iron (Fe) concentration. Used petrol and diesel engine oil samples were analyzed by FT-IR spectroscopy and ICP-OES. PLS models were developed using processed FT-IR spectra as predictor variables and ICP-OES-derived Fe concentrations as response variables. For petrol used oil samples, the optimized model employing 18 latent variables achieved a root mean squared error of 5.02 ppm and a coefficient of determination of 0.97 between measured and predicted Fe concentrations. Model loadings indicated contributions from spectral features associated with soot, oxidation, nitration, antioxidant (AO) depletion, and zinc dialkyldithiophosphate depletion. Combining petrol and diesel samples in a single model reduced predictive performance and increased uncertainty, indicating that their differing degradation pathways cannot be adequately represented by one common latent variable model. The approach does not directly measure Fe and is not intended to replace elemental analysis. Instead, it provides a rapid, low-cost screening tool for identifying samples with potentially elevated wear metal concentrations and prioritizing them for confirmatory analysis.

Keywords: engine oil; internal combustion engine (ICE); wear; Fourier-transformed infrared spectroscopy (FT-IR); partial least squares (PLS) regression

1. Introduction

Lubricants fulfil several key roles in technical systems, such as cooling, transport of additives and degradation products, and corrosion protection, just to name a few, but wear reduction is their primary purpose. Wear—the unwanted loss of material from component surfaces—shortens the service life of individual machine elements and, consequently, of the overall system. This increases the need for maintenance, component replacement, or, in severe cases, remanufacturing of the entire part group. These activities all require financial resources and contribute to material and energy use and, hence, to harmful pollutant emissions.

Lubricants are unique amongst the machine elements—they have a comparatively short service life and are in contact with all the moving parts simultaneously. Thus, their performance is critical. Over the lifetime of an engine oil, additives, such as phenolic and aminic antioxidants, zinc dialkyldithiophosphate (ZDDP) or boron ester antiwears,

Received: 22 June 2026
Revised: 10 August 2026
Accepted: 12 August 2026
Published: 13 August 2026

or the calcium carbonate base reserve depletes [1,2], while degradation products, such as oxidation and nitration species, soot, or organic acids, originate and accumulate [1]. These chemical changes negatively impact engine wear—most notably ZDDP depletion [3,4] and soot accumulation [5–7] largely increase wear rates.

Research on engine oil performance has placed particular emphasis on antiwear additives, especially ZDDP, and friction modifiers such as molybdenum dialkyldithiocarbamates (MoDTC). The central role of ZDDP is reflected in several dedicated reviews [8–10]. Parallel research has evaluated modified or alternative antiwear chemistries, including low-sulfur and low-phosphorus or metal-free additives [11,12], ionic liquids [13,14], and glycerol mono-oleate [15]. Studies on MoDTC have likewise focused on the formation of MoS_2 and its interactions with ZDDP [16–21].

ZDDP reacts with metal surfaces to form protective boundary layers, commonly referred to as tribofilms, which reduce wear under lubricated contact conditions. Their formation is a complex process that generally initiates within the wear track at moderate temperatures and is followed by progressive film growth [22–27]. Several mechanistic models have been proposed to describe both the formation and removal of ZDDP-derived tribofilms [28–32]. A broad range of surface-sensitive techniques have been used to characterize their morphology, elemental and chemical composition, structure, and thickness, including SEM [30], AFM [33,34], EDX [30,34], XPS [29,34], XANES [23], and cross-sectional TEM combined with FIB preparation [35].

In addition to antiwear additive degradation, interactions with particulate contaminants such as soot are an important topic in wear-related research. Several competing mechanisms have been proposed to explain soot-induced wear. One hypothesis is mechanical abrasion, in which soot particles remove tribofilm and substrate material through a three-body wear process [7,36,37] or restrict lubricant replenishment within the contact [38]. A second mechanism involves adsorption of antiwear additives, particularly ZDDP, onto soot particles, thereby reducing their availability for tribofilm formation [39,40]. A third explanation is tribocorrosive wear, in which the sulfide-rich base layer commonly present in ZDDP-derived tribofilms forms but is continuously removed by soot particles [5,6,41,42].

These studies demonstrate that lubricant wear results from complex interactions among additive chemistry, degradation products, particulate contaminants, and surface film formation. Consequently, rapid monitoring methods can provide useful wear screening information, although detailed surface or wear debris analysis remains necessary to identify the underlying wear mechanism.

FT-IR is very commonly used for oil condition monitoring. Standards such as ASTM E2412 [43] and DIN 51453 [44] describe the determination of oxidation, nitration, antiwear additives and soot in detail, amongst other parameters, and additive-specific in-house methods are also available [1]. FT-IR is especially popular, since other determinations, such as total acid number (TAN) [45] or total base number (TBN) [46], require complex infrastructure and chemicals; meanwhile FT-IR is a quick, non-destructive measurement requiring no sample preparation. This is also the case for mass spectrometry (MS), which is a very potent tool in condition monitoring and describing reaction products on the molecular level [47], but is very demanding on the instrumentalization. Other common oil condition monitoring methods include viscometry [48], fuel dilution [49], water content [50] and rust prevention characteristics [51]. Furthermore, mobile FT-IR spectrometers are also available for measurements in the field [52].

The most common methods for determining wear metals in in-service lubricants are inductively coupled plasma optical emission or mass spectrometry (ICP-OES or ICP-MS) and X-ray fluorescence spectroscopy (XRF). Both require comparatively expensive instrumentation and laboratory infrastructure. ICP-based methods either dilute the oil samples in

organic solvents [53] or require microwave-assisted digestion, usually with nitric acid [54], which are time-intensive and make analysis turnaround times longer. XRF requires no sample preparation and, hence, is comparatively faster, but X-ray equipment is usually associated with stronger legal oversight due to radiation safety, which makes these systems more complex in the acquisition. Wear monitoring is possible online for example via radio nucleid technique (RNT) [55] or radio isotope concentration (RIC) methods [56], both involving radiologically activated machine elements. These techniques are highly accurate, but once again the required hardware and preparations are complex and expensive. Complementary wear monitoring approaches include wear sensors, which can be electrical (inductive, capacitive, resistive) [57,58], optical [57,59], or ultrasonic [57] regarding their operating principle. Filter debris analysis and microscopy-based wear debris analysis are also commonly utilized [60]. These methods can provide information on particle size, morphology, or wear mechanisms but generally require specialized instrumentation, interpretation, or system-specific integration.

The aim of this study is the development of a rapid wear screening technique based on the in-service oils FT-IR spectra and modern data science—namely PLS regression. PLS is a multivariate modelling technique that relates a predictor matrix (X) to one or more response variables (y) [61,62]. In the case of a single response variable the method is referred to as PLS1, whereas models involving multiple responses are termed PLS2. In the presented study, PLS1 was performed where X contains the processed FT-IR spectra of the individual oil samples and y corresponds to the Fe content measured via ICP-OES in the engine oil samples. PLS constructs latent variables that maximize the covariance between predictors and response variables, which are subsequently used in a linear regression model.

PLS is conceptually related to principal component analysis (PCA), as both methods produce scores and loadings describing the structure of the predictor space. PCA is already routinely used for the classification of in-service engine oil samples [61,63]. However, PCA identifies directions of maximum variance in X only, whereas PLS incorporates the relationship between predictors and response variables during component extraction. Consequently, the resulting latent variables are optimized for predictive modelling rather than purely for dimensionality reduction. This makes PLS particularly suitable for datasets with large numbers of strongly correlated variables, such as FT-IR spectra, where conventional ordinary least squares regression becomes unstable. Several studies used the combination of FT-IR data with PLS to estimate lubricant parameters. Zho et al. applied PLS on FT-IR attenuated total reflection (ATR) data with various preprocessing methods to model the acid number (AN) in in-service lubricants [64]. Sejkorová et al. used a similar FT-IR ATR/PLS method to model kinematic viscosity [65] and TBN [66]. Macián et al. applied PLS on FT-IR and UV-VIS data of used oils to determine fuel dilution [67]. This shows that the FT-IR PLS approach is very flexible and very potent in lubricant condition monitoring, especially since the infrared spectrum contains a wide variety of information about the chemical composition, contaminations and additives involved. Additionally, machine learning via neural networks can also be applied to multi-parameter oil analysis reports to classify samples and potentially flag critical conditions [68].

To the authors' knowledge, quantitative prediction of elemental wear indicators from used oil FT-IR spectra has received limited attention compared with the established spectroscopic estimation of lubricant condition parameters such as oxidation, acid number, base number, viscosity, soot, or fuel dilution. Unlike these molecular or bulk physicochemical properties, iron is not directly measured by mid-infrared spectroscopy. Any predictive relationship must therefore arise from the multivariate co-evolution of wear with lubricant degradation, additive depletion, contamination, and vehicle operating history. This also defines an important limitation of the approach: model performance depends on the rep-

resentativeness of the calibration dataset and may be influenced by the oil formulation, engine type, service interval, and operating conditions represented therein. The aim of this study was therefore to develop and evaluate a rapid screening approach for estimating Fe concentrations in used engine oils from FT-IR spectra using partial least squares regression. The specific contribution of the present work is the direct prediction of ICP-OES-derived Fe concentrations from full FT-IR spectra, combined with an assessment of how lubricant degradation affects wear rates through the detailed analysis of the derived PLS loadings. To the best of our knowledge, this quick and relatively simple approach to estimating wear from easily accessible spectroscopic data has not yet been presented in the publicly available literature. The proposed method is not intended to replace ICP-OES as a reference technique for elemental analysis. Instead, it is intended to provide a rapid and cost-efficient preliminary assessment that can classify samples according to their expected wear level and identify samples requiring confirmatory elemental or wear debris analysis. Fe was selected as the target wear element because it is commonly associated with the wear of ferrous engine components, including cylinder liners, piston rings, valve train components, bearings, gears, and other steel-containing parts. In used engine oils, increasing Fe concentrations can therefore serve as a broad indicator of metallic component wear. Although elemental analysis alone cannot identify the precise wear source or mechanism, Fe is a highly relevant screening parameter because it is typically among the most abundant wear metals observed in in-service engine oils.

2. Materials and Methods

2.1. Vehicle Field Test Under Real Driving Conditions

Field testing was conducted in prior studies [1,2,54,69] under normal on-road operation of passenger vehicles to obtain lubricant samples representative of real-world service conditions. This involved regular everyday utilization in normal traffic conditions, including both summer and winter operation. Oil samples were collected via the dipstick tube after approximately 5 min of engine idling to ensure adequate mixing and sample homogeneity.

In total, 64 spark ignition (SI or petrol) used oil samples originating from 4 fresh oils and 12 vehicles as well as 12 compression ignition (CI or diesel) used oil samples from 2 fresh oils and 4 vehicles were collected. Vehicle–lubricant combinations are denoted P1–P12 for petrol and D1–D4 for diesel. The dataset includes multiple engine power classes, engine aspirations and service intervals, providing a representative overview of typical European passenger vehicle operating conditions. In total, fresh oils from 4 lubricant manufacturers were considered. All fresh oils contain phenolic and aminic antioxidants, as well as ZDDP antiwear additives. Despite the similar general formulations, several differences are visible between the products. TBN is in the range 6.0–8.4 mgKOH/g, and the corresponding calcium content is between 1100 ppm and 2100 ppm. The applied level of ZDDP is also different between the oil formulations; sulfur content ranges from 1620 ppm to 2230 ppm, phosphor content from 700 ppm to 790 ppm, and zinc content from 830 ppm to 920 ppm. Additionally, boron content, corresponding to boron ester antiwear additives [70], ranges from 0 ppm to 480 ppm. Accordingly, the considered oil chemistries span a representative range of commercially relevant additive strategies, although they do not cover all possible lubricant formulations.

An overview of the vehicles and lubricants investigated is provided in Table 1.

As visible, diesel vehicles are underrepresented compared to their petrol counterparts in the dataset. This is due to the shifting EU passenger vehicle market (see Figure 1), where diesel drivetrains have been losing popularity for multiple years, reaching an all-time-low market share of 8.4% in 2025 according to the European Automobile Manufacturers'

Association (ACEA) [71–73]. Comparatively, pure petrol drivetrains remained relatively popular (26.6% in 2025), and the current dominant technology became hybrid electric vehicles (HEV—34.5%), which mostly contain a petrol ICE. It is also noteworthy that battery electric (BEV) and plug-in hybrid (PHEV) vehicles have only slowly gained further popularity in the EU market since 2023 and seem to stabilize as less common drivetrain configurations. Accordingly, this research is focused more on petrol engines due to both their better availability for studies as well as their higher passenger market relevance. Nevertheless, the limitation on the available number of diesel oil samples greatly affects model building capabilities. Any statistical approach requires an adequate number of observations, which is not given for the diesel population in this case. This is especially problematic, as diesel drivetrains are still dominate the heavy-duty market, e.g., 80.7% of the new van and 93.2% of new truck registrations in 2025 had a diesel drivetrain [73], highlighting that this technology still has its applications—just not in the passenger sector. Accordingly, further data collection, specifically for diesel vehicles, should be carried out.

Table 1. Parameters of utilized vehicles and engine oils for field testing under real driving conditions.

Designation	Engine Power (kW)	SAE Viscosity Class	Engine Type	Displacement (L)	Aspiration	Maximum Torque (Nm)	Compression Ratio (-)	Total Oil Mileage (km)
D1	130	0W-30	diesel	2.0	Turbocharged	380	16.5:1	12,692
D2	140	0W-30	diesel	2.0	Turbocharged	400	15.5:1	7519
D3	140	0W-30	diesel	2.0	Turbocharged	400	15.5:1	9343
D4	84.5	5W-30	diesel	1.6	Turbocharged	270	16.0:1	4296
P1	51	5W-40	petrol	1.2	Naturally aspirated	112	10.5:1	4556
P2	95	5W-30	petrol	2.0	Naturally aspirated	180	10.5:1	30,000
P3	221	0W-30	petrol	2.0	Turbocharged	380	9.3:1	8036
P4	185	0W-30	petrol	2.0	Turbocharged	370	9.6:1	14,694
P5	185	0W-30	petrol	2.0	Turbocharged	370	9.6:1	17,107
P6	185	0W-30	petrol	2.0	Turbocharged	370	9.6:1	6852
P7	221	0W-30	petrol	2.0	Turbocharged	380	9.3:1	5094
P8	221	0W-30	petrol	2.0	Turbocharged	380	9.3:1	2552
P9	155	0W-30	petrol	2.0	Turbocharged	350	9.6:1	1689
P10	155	0W-30	petrol	2.0	Turbocharged	350	9.6:1	1149
P11	155	0W-30	petrol	2.0	Turbocharged	350	9.6:1	1760
P12	88	5W-30	petrol	1.4	Turbocharged	200	9.5:1	19,800

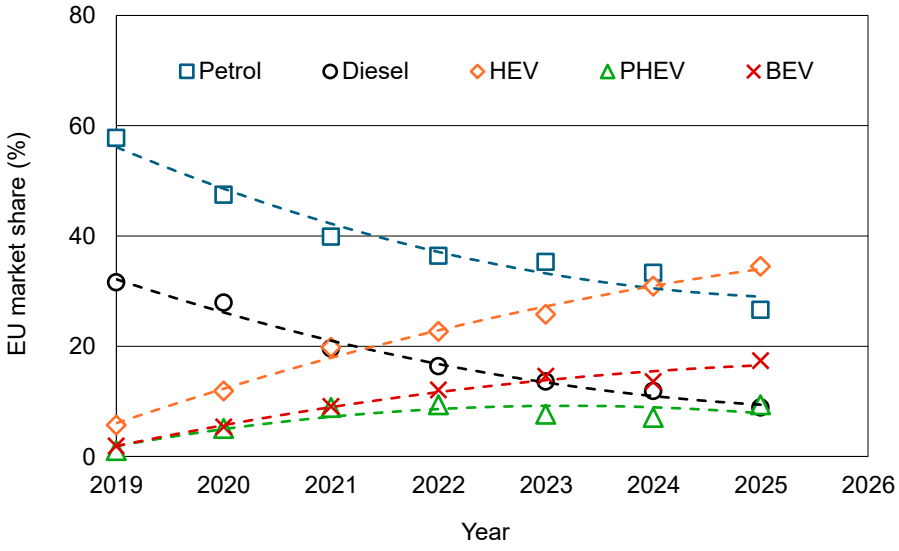

Figure 1. Market share of various drivetrain technologies in the EU amongst new vehicle registrations in 2019–2025, according to the ACEA [71–73].

2.2. Lubricant Analysis

FT-IR measurements were performed using a Tensor II spectrometer (Bruker, Ettlingen, Germany), and the spectra were evaluated with OPUS software (version 8.7.31, Bruker, Ettlingen, Germany). The spectra were recorded over a wavenumber range of 500–4000 cm^{-1} at a spectral resolution of approximately 1.5 cm^{-1}. A dual-channel sample holder was used, with 32 background scans and 32 sample scans collected for each measurement. The oil samples were analyzed in transmission mode using a ZnSe cell with an optical path length of 100 µm.

Elemental concentrations were determined by ICP-OES using a 5800 VDV ICP-OES spectrometer (Agilent Technologies, Santa Clara, CA, USA). Prior to analysis, approximately 0.1 g of each oil sample was subjected to microwave-assisted digestion with nitric acid and hydrogen peroxide in closed vessels. The digested samples were subsequently diluted to a defined volume with ultrapure water.

Quantification was based on external calibration using multi-element standards prepared from commercially available 1000 ppm single-element stock solutions (Carl Roth GmbH, Karlsruhe, Germany). The analyzed elements comprised Al, B, Ba, Ca, Co, Cr, Cu, Fe, K, Li, Mg, Mn, Mo, Na, Ni, P, Pb, S, Sb, Si, Sn, Ti, V, W, and Zn. Calibration solutions were prepared in matrices matched to the respective analytical conditions.

Measurements were conducted in argon plasma using both axial and radial observation modes to accommodate the broad concentration range of the analytes. Multiple emission lines were monitored for each element to reduce the influence of spectral interferences. All samples were measured in triplicate, and the reported concentrations were calculated from the mean responses obtained from the valid emission lines.

Analytical performance was verified using independent multi-element quality control standards measured at the beginning and end of each analytical sequence. Only emission lines yielding concentrations within ±10% of the respective reference values were included in the final evaluation.

2.3. FT-IR Interpretation and Data Preprocessing

FT-IR spectroscopy provides access to a wide range of wear-relevant physicochemical information, including indicators such as ZDDP depletion and soot content. In addition to these established parameters, the spectra contain further information that is not directly evaluated by conventional methods but can be captured through multivariate techniques such as PLS via latent variables.

A model based on FT-IR data therefore offers significant advantages for condition monitoring in terms of both time and cost, as elemental analysis methods such as ICP–OES are comparatively complex and resource-intensive. Moreover, FT-IR measurements can be readily implemented in online monitoring systems, further increasing their practical applicability [43]. For PLS modelling, the measured FT-IR absorbance spectra were used as predictor variables. No baseline correction was applied because the broad increase in absorbance caused by soot represents relevant physical information rather than an instrumental artefact. In used engine oils, soot is conventionally evaluated from the baseline displacement in a feature-free region around 2000 cm^{-1} [43]. Baseline correction or derivative preprocessing would suppress this contribution and was therefore considered unsuitable for the present objective. Spectral regions dominated by complete or near-complete hydrocarbon absorption, namely 2755–3100 cm^{-1} and 1363–1496 cm^{-1}, were excluded. These regions contain limited information on the investigated degradation processes and exhibit comparatively high noise because of the strong absorbance of the hydrocarbon matrix [54]. No further spectral smoothing or derivative transformation was applied. Fol-

lowing the exclusion of these regions, each spectrum comprised 1573 absorbance values for subsequent PLS modelling [54].

Several spectral regions are considered during the model interpretation which correspond to various lubricant degradation mechanisms. Detailed information is available in Table 2.

Table 2. Lubricant specific FT-IR evaluation ranges.

Chemical Species	Evaluation Details	Source
Phenol AOs (depletion)	Peak height at 3650 cm^{-1} over global baseline	In-house method [1]
Amine AOs (depletion)	Peak height at 1515 cm^{-1} over local baseline	In-house method [1]
ZDDP antiwear (depletion)	Highest peak between 927 and 1019 cm^{-1} over local baseline	In-house method [1]
Oxidation products (accumulation)	Peak height at 1710 cm^{-1} over global baseline	In-house method [1]
Nitration products (accumulation)	Peak height at 1630 cm^{-1} over local baseline	DIN 51453 [44]
Soot (accumulation)	Baseline shift at 2000 cm^{-1}	ASTM E2412 [43]
Water (accumulation)	Area 3150–3500 cm^{-1}	ASTM E2412 [43]
Diesel contamination (accumulation)	Area 805–815 cm^{-1}	ASTM E2412 [43]
Petrol contamination (accumulation)	Area 745–755 cm^{-1}	ASTM E2412 [43]

Finally, the processed spectra were exported from OPUS and converted into numerical format for subsequent multivariate analysis.

2.4. Partial Least Squares Regression

Initial investigations on modelling engine wear based on FT-IR spectral data were previously reported in [54], focusing on a petrol-only dataset. The present work extends this approach to mixed petrol and diesel samples. PLS models were implemented in Python® (version 3.13.2) using the scikit-learn library (version 1.7) [74]. The dataset was divided into training (80%) and test (20%) subsets using a stratified sampling approach based on the response variable (Fe content) to ensure representation across the full measured concentration range. This approach ensures that low, medium and high Fe content samples are represented in the test data; hence, the model evaluation considers the whole available response variable range. In doing so, a fixed random seed was used to ensure reproducibility.

Hyperparameter tuning was performed on the training dataset using the GridSearchCV function of SciKit learn, with five-fold cross-validation. The training data were divided into five subsets of approximately equal size. For each candidate number of latent variables, the model was fitted five times, using four folds for training and the remaining fold for validation in each iteration, so that every fold served once as the validation set. The resulting validation errors were averaged across the five iterations and recorded.

The optimal number of latent variables was determined by minimizing the cross-validated root mean squared error (RMSE) [61,62]. Selecting the number of components based on the validation error provides an effective safeguard against both underfitting and overfitting [62]. Models employing too few components are unable to adequately capture the underlying covariance structure of the data, whereas excessively complex

models tend to incorporate noise rather than chemically meaningful information, resulting in increased validation errors. Selecting the number of components based on the minimum cross-validated RMSE provides an objective and quantitative criterion for model selection, thereby reducing the risk of both underfitting and overfitting and promoting an appropriate model complexity.

Following hyperparameter optimization, the final model was trained on the full training set and evaluated using the independent test dataset. Model stability was assessed using bootstrap resampling of the training data (1000 iterations). Here, the training dataset is repeatedly resampled with replacement, and the complete modelling procedure is repeated, resulting in slightly different models for each bootstrap iteration. Predictions for the original test samples are subsequently aggregated to obtain the median prediction and corresponding confidence bounds. The resulting confidence intervals therefore reflect the stability of the modelling procedure under resampling rather than analytical measurement uncertainty.

Confidence intervals (in this case 90%) describe the uncertainty associated with the model estimate itself, representing the range in which the expected mean prediction would fall if the modelling procedure were repeated. Figure 2 illustrates the PLS workflow.

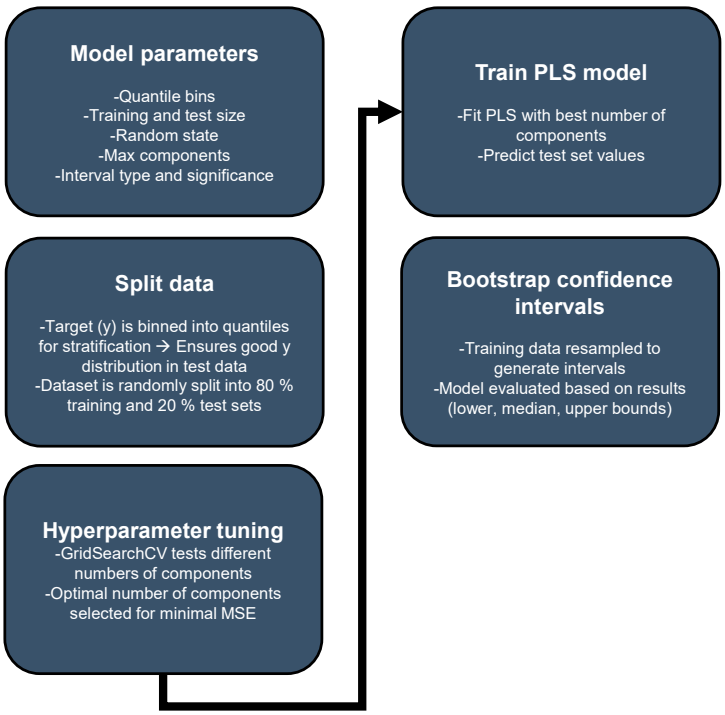

Figure 2. Illustration of the PLS workflow.

3. Results and Discussion

Figure 3 shows the Fe content of the engine oil samples as a function of the mileage. It is well visible that Fe increases over the mileage of the oil samples as engine wear propagates. However, no clear trend is observable between Fe and mileage, since engine wear is influenced by several parameters, so a simple linear regression is not suitable for prediction. As petrol and diesel populations are shown separately, it is also visible that diesel engines tend to produce higher Fe content compared to petrol engines. This is usually associated with the higher soot loading in diesel engines [5,54].

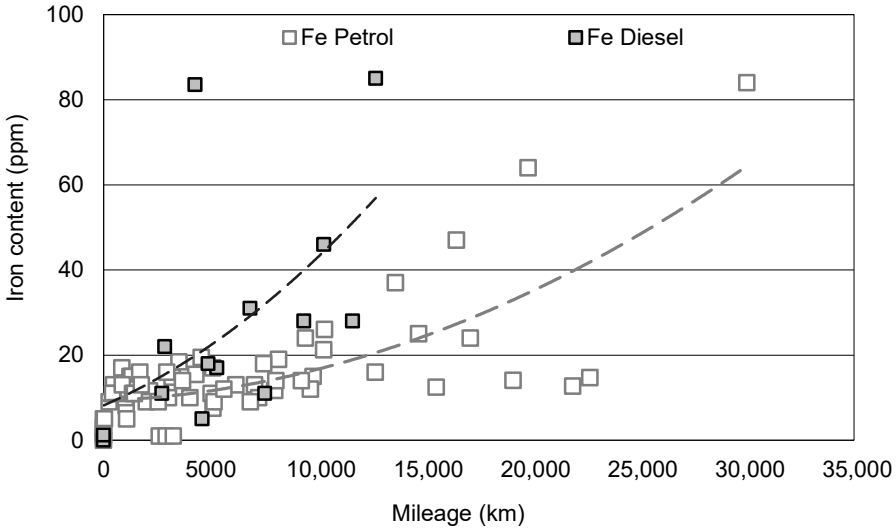

Figure 3. Iron content of the used engine oils determined by ICP-OES. Petrol and diesel populations are shown separately.

3.1. Petrol Used Oil Samples—Petrol Model

Initially, PLS was attempted on the petrol oil samples only, as data availability is better for this population (64 observations).

Figure 4 summarizes the key parameters of the petrol model. Part (a) presents the results of the hyperparameter tuning, showing the RMSE as a function of the number of components. The optimal model complexity was determined by minimizing the RMSE, thereby balancing underfitting and overfitting. In the present case, 18 components were selected, resulting in a RMSE of 5.02 ppm, corresponding to approximately 10% of the iron concentration range investigated.

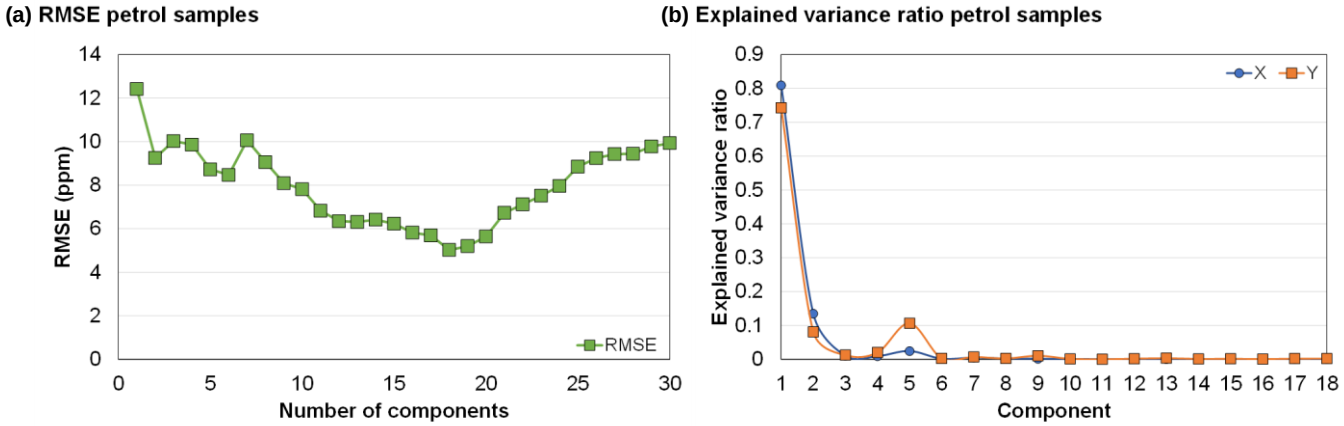

Figure 4. (**a**): Hyperparameter tuning of the petrol model—RMSE as a function of number of components. (**b**): Explained X and y variance ratios by the components of the final petrol model.

Panel (b) shows the explained variance ratios for both X and y. It should be noted that PLS maximizes the covariance between predictor and response variables rather than the variance in X alone. The first two components account for the majority of the explained variance in both X (94.4%) and y (82.4%) and were therefore considered sufficient for interpretation of the model loadings. However, it is also noted that component 5 shows a slightly elevated explained variance ratio.

Figure 5a illustrates the predictive performance of the PLS model by comparing measured Fe concentrations (ICP–OES) with the median predictions obtained from 1000 bootstrap iterations. The error bars represent 90% confidence intervals derived from

the bootstrap distributions. As each iteration involves a new randomized train–test split, individual samples may be included in either the training or test set across different runs. Accordingly, the reported confidence intervals reflect model stability under resampling rather than analytical measurement uncertainty.

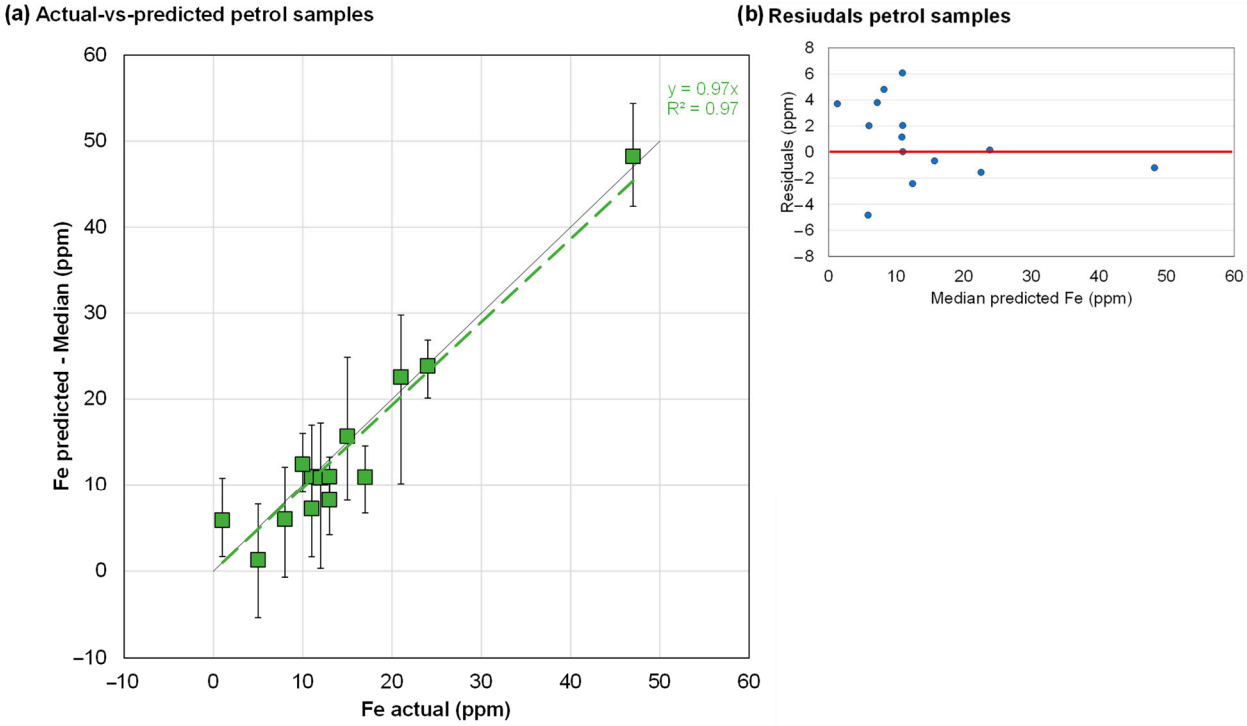

Figure 5. (**a**): Actual vs. median predicted Fe values of the petrol model. The green dashed line represents the linear regression fit. Error bars indicate 90% confidence intervals based on 1000 bootstrap iterations. (**b**): Residuals of the petrol model based on the median prediction from 1000 bootstrap iterations. The red line indicates zero residuals.

Overall, the model exhibits strong predictive performance within the investigated concentration range. Linear regression between measured and predicted values yields a slope of 0.97, indicating minimal systematic bias, and a coefficient of determination (R^2) of 0.97, confirming low residual error. The mean prediction error is approximately 5.0 ppm, while deviations exceeding 10 ppm occur in only two out of 28 evaluations. These results demonstrate that iron content—and thus a key indicator of tribological performance—can be reliably estimated from FT-IR spectra. Figure 5b shows the residuals of the petrol model test set. Residuals are distributed approximately symmetrically around zero, and no pronounced concentration-dependent trend is observed across the investigated Fe concentration range. Furthermore, the residual spread does not increase substantially at higher predicted Fe contents, indicating stable predictive performance over the investigated range. These findings provide additional evidence that the model does not exhibit obvious systematic bias or overfitting.

Figure 6 presents the X-loadings of components 1 and 2. As the response variable (Fe concentration) is univariate, the corresponding y-loadings provide limited additional insight and are therefore not shown. Instead, the X-loadings are used to identify the spectral features contributing to the model. For reference, characteristic FT-IR evaluation regions are indicated, including water, soot, diesel and gasoline, as well as oxidation, nitration, phenolic and aminic antioxidants, and ZDDP-related signals. Spectral gaps correspond to excluded hydrocarbon absorption regions (see Table 2 for evaluation details).

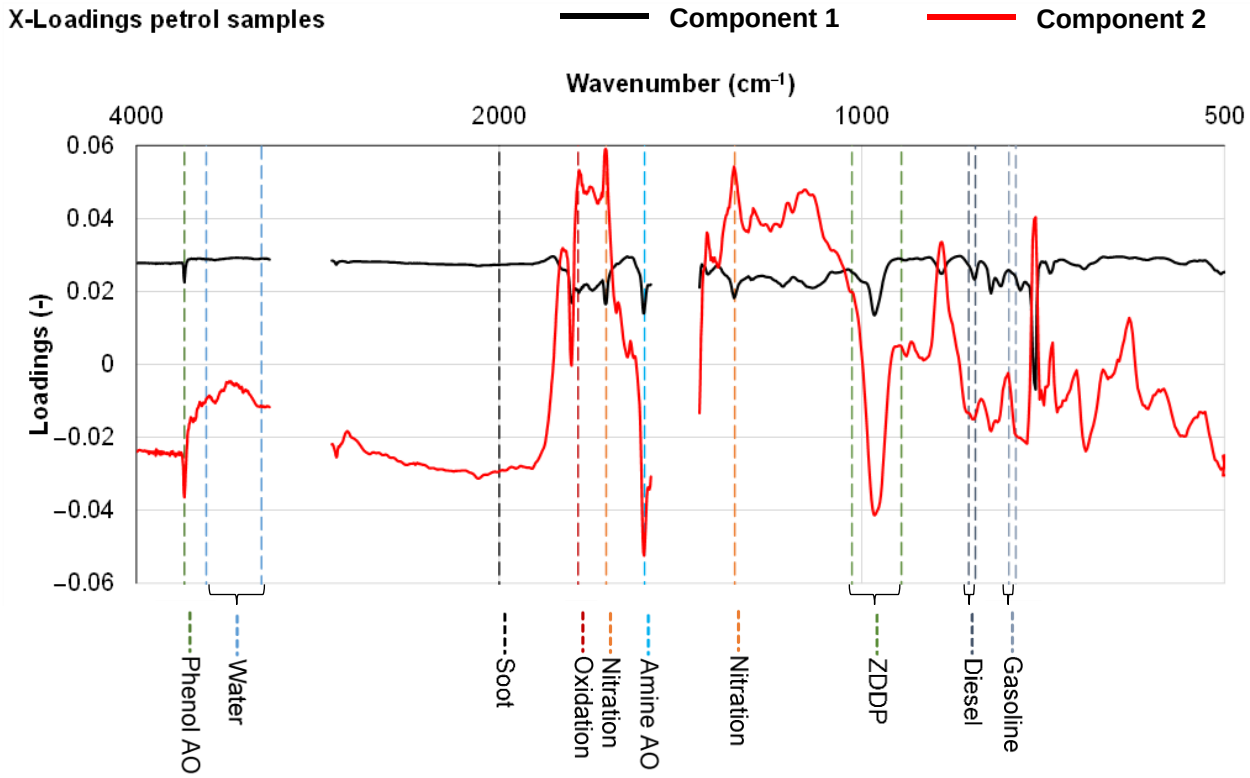

Figure 6. X-loadings of the petrol model (the x-axis is displayed on a base 2 logarithmic scale). Relevant spectral regions highlighted based on Table 2.

Component 1 exhibits broadly uniform and elevated contributions across the entire wavenumber range, which is characteristic of soot-related baseline absorption. This characteristic "baseline shift" emerges from the soot particles, as they are absorbing across the whole wavenumber-range. The reason for the standard evaluation at 2000 cm^{-1} [43] is simply the absence of other dominant spectral features in this region.

In contrast, component 2 highlights distinct spectral regions associated with lubricant degradation processes. The large contributions of degradation product accumulation, most notably oxidation and nitration, are well visible. Additionally, additive depletion, namely phenolic and aminic antioxidants as well as ZDDP antiwear, also contribute strongly to the model. In general, component 2 depicts the typical chemical changes associated with thermo-oxidative oil degradation.

These results indicate that the PLS model captures the key physicochemical information governing oil degradation. A key advantage of this approach is that the overall lubricant condition can be represented by a single predicted variable, thereby avoiding the need for separate evaluation of multiple individual degradation parameters, hence greatly reducing the time and effort of the interpretation.

3.2. All Used Oil Samples—Mixed Model

Subsequently, PLS was also attempted on the whole oil sample dataset. Here the 64 petrol and 12 diesel observations were handled together, resulting in a mixed model.

The parameters of the mixed model are shown in Figure 7a and b, respectively. The hyperparameter tuning (a) indicated a minimal RMSE of 4.59 ppm at 15 components. The explained variance ratio of the corresponding model is shown in Figure 7b, where the first two components explain 95.2% of the X and 69.4% of the y variance. Compared to the petrol model, the number of components and explained X variance ratios are similar, but the explained y variance ratio decreased considerably from 82.4% once the diesel

used oil samples are also included. This indicates that the mixed model was less able to capture the underlying tribochemical processes. Additionally, the explained y variance ratio contribution of component 5 is high at 23.7%, indicating that this latent variable carries an elevated weight when diesel used oils are also included in the data.

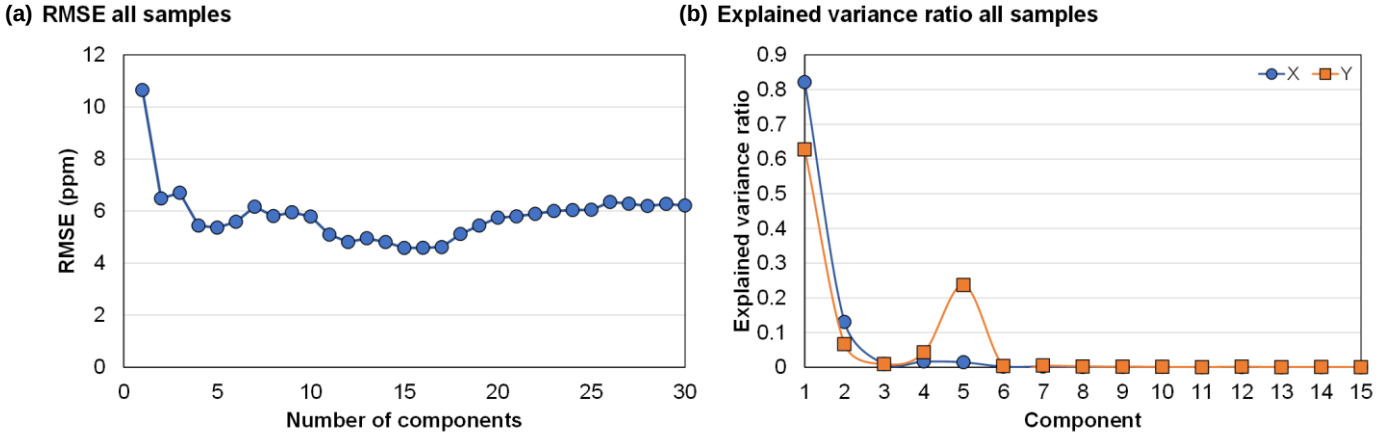

Figure 7. (**a**): Hyperparameter tuning of the mixed model—RMSE as a function of number of components. (**b**): Explained X and y variance ratios by the components of the final mixed model.

Figure 8a evaluates the predictive performance of the mixed PLS model, with petrol and diesel samples in the test set highlighted separately. Overall, the mixed model performs worse than the petrol-only model. A linear regression based on the petrol samples alone already shows increased systematic bias (slope = 0.91) and reduced goodness of fit (R^2 = 0.91), indicating a deterioration in predictive accuracy.

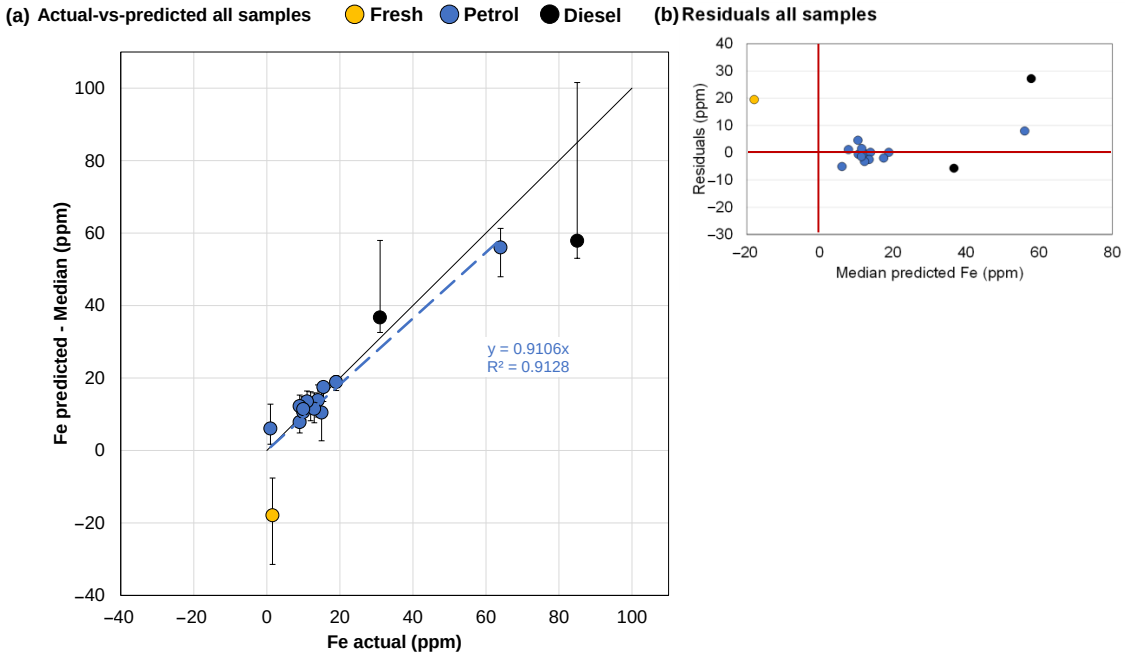

Figure 8. (**a**): Actual vs. median predicted Fe values of the mixed model. The blue dashed line represents the linear regression fit. Error bars indicate 90% confidence intervals based on 1000 bootstrap iterations. (**b**): Residuals of the mixed model based on the median prediction from 1000 bootstrap iterations. The red lines indicate zero residuals.

The diesel samples deviate markedly from the regression line, particularly at higher Fe concentrations. In addition, substantially broader confidence intervals are observed

(up to 25 ppm and 48 ppm), reflecting increased prediction uncertainty. Additionally, one fresh oil sample exhibited suboptimal predictive performance, resulting in a negative predicted Fe value. The residual analysis presented in Figure 8b revealed that the residuals of most petrol observations are distributed closely around zero without a pronounced concentration-dependent trend. One fresh oil sample exhibited a comparatively large residual of approximately 19 ppm and a diesel sample 27 ppm, highlighting the general instability of the prediction for the diesel population and the general limitations of the mixed model.

These results indicate reduced model stability and suggest that the PLS model is unable to consistently capture degradation patterns when both fuel types are combined. This behaviour is partly attributable to the smaller number of diesel observations; however, it is primarily driven by fundamental differences in degradation mechanisms. Petrol engine oils are typically dominated by oxidative degradation, nitration, and additive depletion under relatively lower air–fuel ratios [2,63,69]. In contrast, diesel engines exhibit limited fuel evaporation due to the higher boiling range of diesel fuel, leading to poorer mixture homogeneity and increased soot formation [2]. Previous field studies attributed higher importance to soot-based diesel-typical wear compared to oxidation-based petrol-typical processes [2,5], where it was also shown that wear returns to levels comparable to fresh oils once soot is removed by ultracentrifugation [5]. These fundamental differences in tribochemical pathways explain the reduced performance of the mixed model and highlight that a single global PLS model is insufficient to describe both petrol and diesel oil degradation within a unified latent variable framework.

Figure 9 displays the X-loadings of component 1 and 2 for the mixed model, where similar considerations to the petrol model can be made. Component 1 is mostly capturing soot (baseline shift); component 2 contains the typical oxidative degradation indicators such as oxidation, nitration and additive depletion markers (antioxidant and antiwear additives). In this regard, the mixed model is similar to the petrol version.

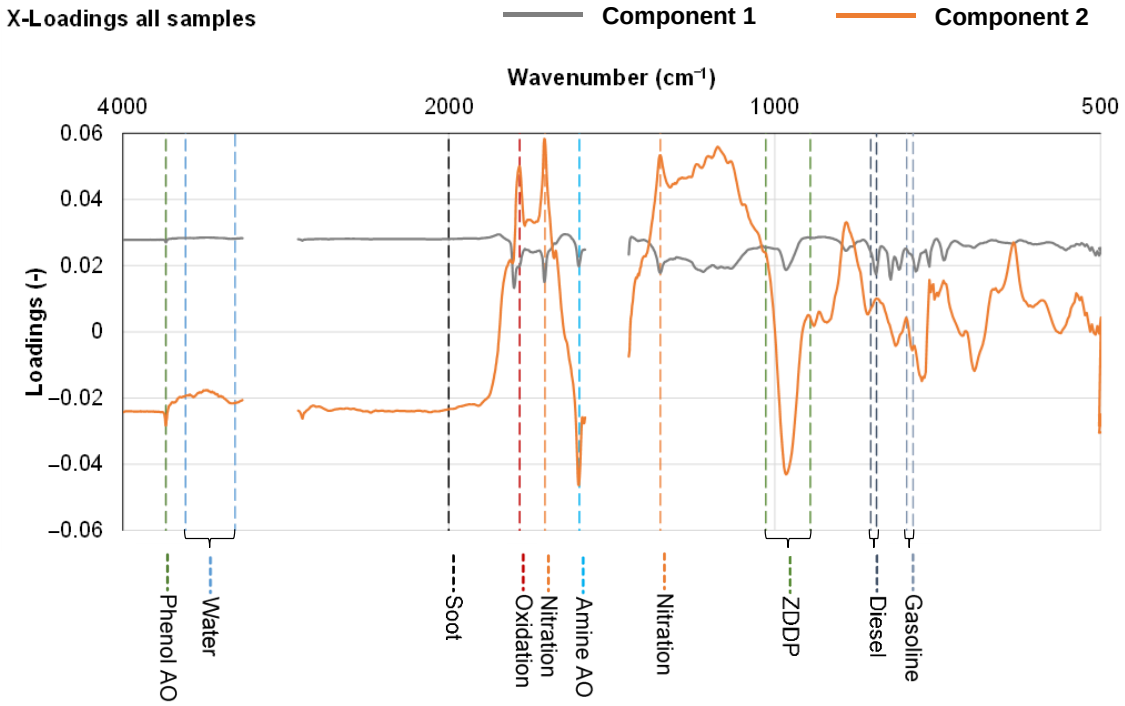

Figure 9. X-loadings of the mixed model (the x-axis is displayed on a base 2 logarithmic scale). Relevant spectral regions highlighted based on Table 2.

Figure 10 additionally shows the X-loadings of component 5 due to its relatively high explained y variance ratio. This phenomenon was also visible in the petrol only model to a lesser extent (see Figure 4). Here, strong contributions of the gasoline- and diesel fuel-related regions are visible, indicating that this component could be sensitive to fuel dilution, hence the elevated weighting once both petrol and diesel engine oils are considered. The need for higher-order components to adequately cover the y-variance reflects additional variance introduced by diesel samples, which contributes to reduced model interpretability and stability. Hence, the mixed model displayed overall inferior predictive performance compared to the petrol model, indicating that different tribochemical processes are hard to assess by a single PLS model. An accurate diesel model could very likely be constructed if a suitable dataset were available.

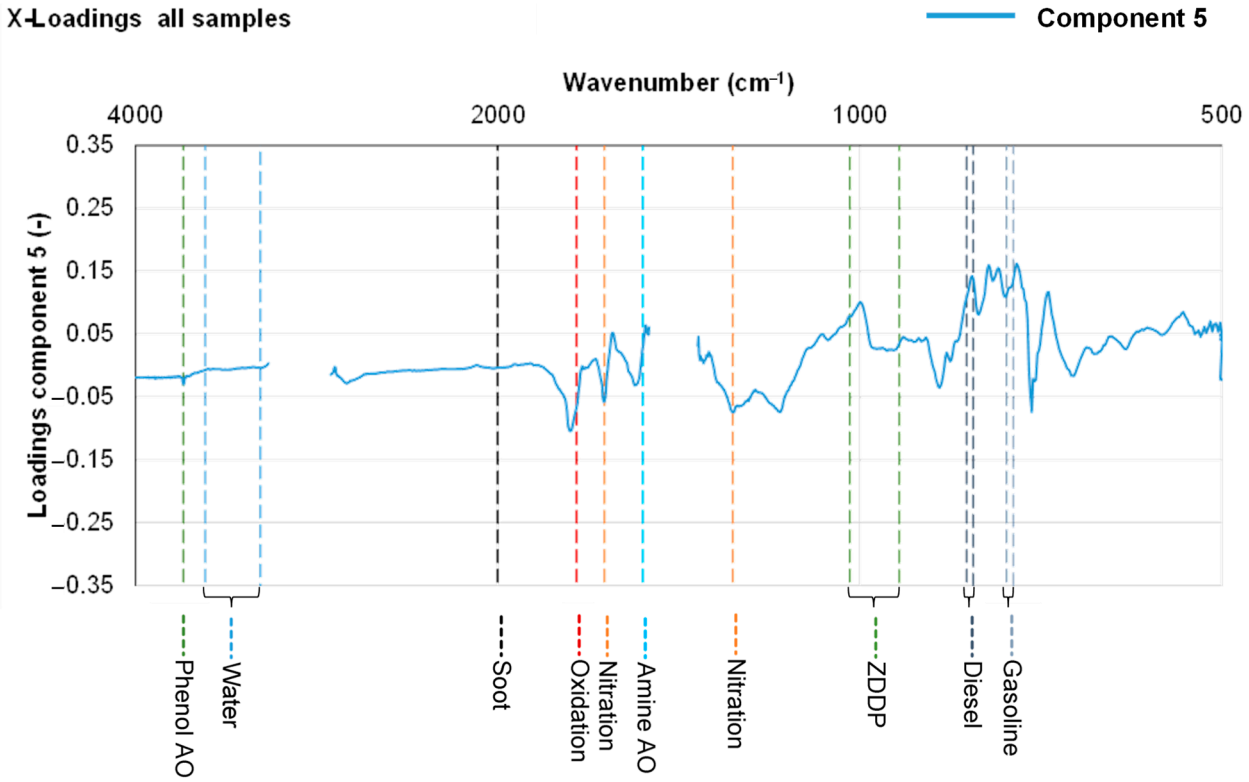

Figure 10. Further X-loadings of the mixed model (the x-axis is displayed on a base 2 logarithmic scale). Relevant spectral regions highlighted based on Table 2.

4. Conclusions and Outlook

PLS regression was applied to FT-IR spectra of 64 petrol and 12 diesel used oil samples to model Fe content as a wear indicator determined by ICP-OES. The petrol-only model demonstrated good predictive performance with a RMSE of 5.02 ppm and an R^2 value of 0.97. Analysis of the X-loadings indicated that soot-related spectral features, oxidative degradation, and additive depletion are the dominant contributors associated with wear prediction. This highlights that cost-efficient analytical techniques such as FT-IR can be effectively combined with accessible data-driven methods such as PLS to enable rapid assessment of wear behaviour in internal combustion engines.

When both petrol and diesel samples were included, predictive performance decreased considerably. In particular, predictions for diesel samples became unreliable, with confidence intervals reaching up to approximately 50 ppm. This indicates a fundamental limitation of the approach: while similar spectral features are present, the relationship between these features and wear differs between petrol and diesel systems. As a result,

a single mixed model cannot adequately capture the underlying tribochemical processes. Still, the development of a diesel-specific model seems feasible, where the only real limitation is the data availability. Accordingly, further diesel-field studies should be conducted, especially focusing on heavy-duty applications, to derive the necessary spectroscopic and elemental composition results.

These findings suggest that tribological modelling using spectroscopic data—although applicable for various oil chemistries—must remain fuel-specific. With the anticipated introduction of alternative, carbon-neutral fuels such as hydrogen, ammonia, and methanol, this distinction is expected to become even more critical, and the development of specific models for each fuel type and application is expected. As wear is influenced by several parameters, most notably additive depletion and degradation products which arise from lubricant–fuel interactions, capturing every aspect for every possible combination of fuels and lubricant formulations seems overly complex. This, however, is not a major technical challenge. FT-IR is commonly available and cost-efficient; hence, it is one of the most applied oil condition monitoring methods. Since the involved calculations of model training are not resource-intensive and can be performed on free, open-source software just as in this case, any operator could easily fit equipment and fuel-specific models once around 50 oil samples are collected in the course of routine oil condition monitoring. Also, retraining the models once more data becomes available is similarly rapid and can be done under an hour on any modern office computer.

Nevertheless, data-driven approaches can significantly enhance condition monitoring, since they offer considerable advantages in analysis time and cost. The presented approach can return an estimated Fe content within a few minutes without requiring sample digestion, calibration standards or elemental analysis, as both the FT-IR measurement and the calculations are very rapid. Meanwhile, elemental analysis would take from several hours to days depending on equipment availability. A further benefit is the prevalence of mobile FT-IR spectrometer which can be used in the field without any external infrastructure, hence enabling operators to carry out a quick assessment on wear levels in various environments directly next to the equipment during routine checks. A possible approach for fleet operators would be the implementation of a quick regular oil level check combined with a mobile FT-IR measurement to flag potentially problematic lubricant conditions—not only considering wear but also other commonly calculated parameters such as oxidation, viscosity and TBN as well. This would enhance the robustness of vehicle and equipment operation as problems would be highlighted early, and corrective maintenance action could be taken before major engine damage occurs. For large engines and stationary applications, the integration of a FT-IR sensor into the oil circuit is also a possible approach. This would enable constant monitoring of the oil condition and, coupled with advanced data-driven approaches, could optimize maintenance planning by a great extent. However, the complexity and cost of this approach are only justifiable for industrial machinery.

With larger and more diverse datasets, future studies could additionally evaluate nonlinear and ensemble machine learning approaches and extend the modelling strategy to further wear metals and various other lubricant parameters; however, rigorous cross-validation and external validation would be required to determine whether their increased complexity provides a genuine advantage over the interpretable PLS approach.

Author Contributions: Conceptualization, A.A., C.B. and G.V.; methodology, A.A. and G.V.; software, A.A.; validation, G.V.; formal analysis, A.A.; investigation, A.A.; resources, C.B. and M.F.; data curation, A.A.; writing—original draft preparation, A.A. and G.V.; writing—review and editing, C.B. and M.F.; visualization, A.A.; supervision, C.B. and M.F.; project administration, C.B. and M.F.; funding acquisition, M.F. All authors have read and agreed to the published version of the manuscript.

Funding: The presented results were realized as part of the COMET Centre InTribology (FFG no. 906860), a project of the "Excellence Centre for Tribology" (AC2T research GmbH). InTribology is funded within the COMET—Competence Centres for Excellent Technologies—programme by the federal ministries BMIMI and BMWET as well as the federal states of Niederösterreich and Vorarlberg based on financial support from the project partners involved. COMET is managed by the Austrian Research Promotion Agency (FFG).

Data Availability Statement: The original contributions presented in this study are included in the article. Further inquiries can be directed to the corresponding author.

Acknowledgments: During the preparation of this manuscript, the authors used ChatGPT version 5.6 Sol (OpenAI) for the purposes of English language editing and the literature research support. The authors have reviewed and edited the output and take full responsibility for the content of this publication.

Conflicts of Interest: All authors are employed by AC2T research GmbH.

Abbreviations

The following abbreviations are used in this manuscript:

AN	Acid number
AO	Antioxidant
ASTM	ASTM International
ATR	Attenuated total reflectance
BEV	Battery electric vehicle
CI	Compression ignition
DIN	Deutsches Institut für Normung
Fe	Iron
FT-IR	Fourier-transform infrared spectroscopy
HEV	Hybrid electric vehicle
ICE	Internal combustion engine
ICP-MS	Inductively coupled plasma mass spectrometry
ICP-OES	Inductively coupled plasma optical emission spectroscopy
MS	Mass spectrometry
MSE	Mean squared error
PCA	Principal component analysis
PHEV	Plug-in hybrid electric vehicle
PLS or PLSR	Partial least squares
RIC	Radio isotope concentration
RMSE	Root mean squared error
SAE	Society of Automotive Engineers
SI	Spark ignition
TAN	Total acid number
TBN	Total base number
UV-Vis	Ultraviolet-visible spectroscopy
XRF	X-ray fluorescence
ZnSe	Zinc selenide
ZDDP	Zinc dialkyldithiophosphate

References

1. Dörr, N.; Agocs, A.; Besser, C.; Ristić, A.; Frauscher, M. Engine Oils in the Field: A Comprehensive Chemical Assessment of Engine Oil Degradation in a Passenger Car. *Tribol. Lett.* **2019**, *67*, 68. [CrossRef]
2. Agocs, A.; Nagy, A.L.; Tabakov, Z.; Perger, J.; Rohde-Brandenburger, J.; Schandl, M.; Besser, C.; Dörr, N. Comprehensive Assessment of Oil Degradation Patterns in Petrol and Diesel Engines Observed in a Field Test with Passenger Cars—Conventional Oil Analysis and Fuel Dilution. *Tribol. Int.* **2021**, *161*, 107079. [CrossRef]

3. Agocs, A.; Besser, C.; Brenner, J.; Budnyk, S.; Frauscher, M.; Dörr, N. Engine Oils in the Field: A Comprehensive Tribological Assessment of Engine Oil Degradation in a Passenger Car. *Tribol. Lett.* **2022**, *70*, 28. [CrossRef]
4. Fuller, M.L.S.; Kasrai, M.; Bancroft, G.M.; Fyfe, K.; Tan, K.H. Solution Decomposition of Zinc Dialkyl Dithiophosphate and Its Effect on Antiwear and Thermal Film Formation Studied by X-Ray Absorption Spectroscopy. *Tribol. Int.* **1998**, *31*, 627–644. [CrossRef]
5. Agocs, A.; Frauscher, M.; Ristic, A.; Dörr, N. Impact of Soot on Internal Combustion Engine Lubrication—Oil Condition Monitoring, Tribological Properties, and Surface Chemistry. *Lubricants* **2024**, *12*, 401. [CrossRef]
6. Kontou, A.; Southby, M.; Morgan, N.; Spikes, H.A. Influence of Dispersant and ZDDP on Soot Wear. *Tribol. Lett.* **2018**, *66*, 157. [CrossRef]
7. Green, D.A.; Lewis, R. The Effects of Soot-Contaminated Engine Oil on Wear and Friction: A Review. *Proc. Inst. Mech. Eng. Part D J. Automob. Eng.* **2008**, *222*, 1669–1689. [CrossRef]
8. Nicholls, M.A.; Do, T.; Norton, P.R.; Kasrai, M.; Bancroft, G.M. Review of the Lubrication of Metallic Surfaces by Zinc Dialkyl-Dithiophosphates. *Tribol. Int.* **2005**, *38*, 15–39. [CrossRef]
9. Spikes, H. The History and Mechanisms of ZDDP. *Tribol. Lett.* **2004**, *17*, 469–489. [CrossRef]
10. Xue, Q.; Liu, W. Tribochemistry and the Development of AW and EP Oil Additives—A Review. *Lubr. Sci.* **1994**, *7*, 81–92. [CrossRef]
11. Rastogi, R.B.; Maurya, J.L.; Jaiswal, V. Low Sulfur, Phosphorus and Metal Free Antiwear Additives: Synergistic Action of Salicylaldehyde N(4)-Phenylthiosemicarbazones and Its Different Derivatives with Vanlube 289 Additive. *Wear* **2013**, *297*, 849–859. [CrossRef]
12. Spikes, H. Low- and Zero-sulphated Ash, Phosphorus and Sulphur Anti-wear Additives for Engine Oils. *Lubr. Sci.* **2008**, *20*, 103–136. [CrossRef]
13. Qu, J.; Luo, H.; Chi, M.; Ma, C.; Blau, P.J.; Dai, S.; Viola, M.B. Comparison of an Oil-Miscible Ionic Liquid and ZDDP as a Lubricant Anti-Wear Additive. *Tribol. Int.* **2014**, *71*, 88–97. [CrossRef]
14. Sharma, V.; Doerr, N.; Erdemir, A.; Aswath, P.B. Interaction of Phosphonium Ionic Liquids with Borate Esters at Tribological Interfaces. *RSC Adv.* **2016**, *6*, 53148–53161. [CrossRef]
15. Matta, C.; De Barros Bouchet, M.I.; Le-Mogne, T.; Vachet, B.; Martin, J.M.; Sagawa, T. Tribochemistry of Tetrahedral Hydrogen-free Amorphous Carbon Coatings in the Presence of OH-containing Lubricants. *Lubr. Sci.* **2008**, *20*, 137–149. [CrossRef]
16. Gorbatchev, O.; Bouchet, M.I.D.B.; Martin, J.M.; Léonard, D.; Le-Mogne, T.; Iovine, R.; Thiebaut, B.; Héau, C. Friction Reduction Efficiency of Organic Mo-Containing FM Additives Associated to ZDDP for Steel and Carbon-Based Contacts. *Tribol. Int.* **2016**, *99*, 278–288. [CrossRef]
17. Rai, Y.; Neville, A.; Morina, A. Transient Processes of MoS 2 Tribofilm Formation under Boundary Lubrication. *Lubr. Sci.* **2016**, *28*, 449–471. [CrossRef]
18. Spikes, H. Friction Modifier Additives. *Tribol. Lett.* **2015**, *60*, 5. [CrossRef]
19. Morina, A.; Neville, A.; Priest, M.; Green, J.H. ZDDP and MoDTC Interactions and Their Effect on Tribological Performance—Tribofilm Characteristics and Its Evolution. *Tribol. Lett.* **2006**, *24*, 243–256. [CrossRef]
20. Topolovec Miklozic, K.; Graham, J.; Spikes, H. Chemical and Physical Analysis of Reaction Films Formed by Molybdenum Dialkyl-Dithiocarbamate Friction Modifier Additive Using Raman and Atomic Force Microscopy. *Tribol. Lett.* **2001**, *11*, 71–81. [CrossRef]
21. Martin, J.; Grossiord, C.; Varlot, K.; Vacher, B.; Igarashi, J. Synergistic Effects in Binary Systems of Lubricant Additives: A Chemical Hardness Approach. *Tribol. Lett.* **2000**, *8*, 193–201. [CrossRef]
22. Zhang, J.; Spikes, H. On the Mechanism of ZDDP Antiwear Film Formation. *Tribol. Lett.* **2016**, *63*, 24. [CrossRef]
23. Varlot, K.; Kasrai, M.; Martin, J.M.; Vacher, B.; Bancroft, G.M.; Yamaguchi, E.S.; Ryason, P.R. Antiwear Film Formation of Neutral and Basic ZDDP: Influence of the Reaction Temperature and of the Concentration. *Tribol. Lett.* **2000**, *8*, 9–16. [CrossRef]
24. Fujita, H.; Spikes, H.A. The Formation of Zinc Dithiophosphate Antiwear Films. *Proc. Inst. Mech. Eng. Part J J. Eng. Tribol.* **2004**, *218*, 265–278. [CrossRef]
25. Taylor, L.; Dratva, A.; Spikes, H.A. Friction and Wear Behavior of Zinc Dialkyldithiophosphate Additive. *Tribol. Trans.* **2000**, *43*, 469–479. [CrossRef]
26. Suominen Fuller, M.L.; Rodriguez Fernandez, L.; Massoumi, G.R.; Lennard, W.N.; Kasrai, M.; Bancroft, G.M. The Use of X-ray Absorption Spectroscopy for Monitoring the Thickness of Antiwear Films from ZDDP. *Tribol. Lett.* **2000**, *8*, 187–192. [CrossRef]
27. Palacios, J.M. Thickness and Chemical Composition of Films Formed by Antimony Dithiocarbamate and Zinc Dithiophosphate. *Tribol. Int.* **1986**, *19*, 35–39. [CrossRef]
28. Ghanbarzadeh, A.; Piras, E.; Nedelcu, I.; Brizmer, V.; Wilson, M.C.T.; Morina, A.; Dowson, D.; Neville, A. Zinc Dialkyl Dithiophosphate Antiwear Tribofilm and Its Effect on the Topography Evolution of Surfaces: A Numerical and Experimental Study. *Wear* **2016**, *362–363*, 186–198. [CrossRef]

29. Morina, A.; Neville, A. Tribofilms: Aspects of Formation, Stability and Removal. *J. Phys. D Appl. Phys.* **2007**, *40*, 5476–5487. [CrossRef]
30. Morina, A.; Neville, A. Understanding the Composition and Low Friction Tribofilm Formation/Removal in Boundary Lubrication. *Tribol. Int.* **2007**, *40*, 1696–1704. [CrossRef]
31. de Barros'Bouchet, M.I.; Martin, J.M.; Le-Mogne, T.; Vacher, B. Boundary Lubrication Mechanisms of Carbon Coatings by MoDTC and ZDDP Additives. *Tribol. Int.* **2005**, *38*, 257–264. [CrossRef]
32. Fujita, H.; Spikes, H.A. Study of Zinc Dialkyldithiophosphate Antiwear Film Formation and Removal Processes, Part II: Kinetic Model. *Tribol. Trans.* **2005**, *48*, 567–575. [CrossRef]
33. Gosvami, N.N.; Bares, J.A.; Mangolini, F.; Konicek, A.R.; Yablon, D.G.; Carpick, R.W. Mechanisms of Antiwear Tribofilm Growth Revealed in Situ by Single-Asperity Sliding Contacts. *Science* **2015**, *348*, 102–106. [CrossRef] [PubMed]
34. Parsaeian, P.; Ghanbarzadeh, A.; Van Eijk, M.C.P.; Nedelcu, I.; Neville, A.; Morina, A. A New Insight into the Interfacial Mechanisms of the Tribofilm Formed by Zinc Dialkyl Dithiophosphate. *Appl. Surf. Sci.* **2017**, *403*, 472–486. [CrossRef]
35. Dawczyk, J.; Ware, E.; Ardakani, M.; Russo, J.; Spikes, H. Use of FIB to Study ZDDP Tribofilms. *Tribol. Lett.* **2018**, *66*, 155. [CrossRef]
36. Vyavhare, K.; Bagi, S.; Patel, M.; Aswath, P.B. Impact of Diesel Engine Oil Additives-Soot Interactions on Physiochemical, Oxidation, and Wear Characteristics of Soot. *Energy Fuels* **2019**, *33*, 4515–4530. [CrossRef]
37. Gautam, M.; Chitoor, K.; Durbha, M.; Summers, J.C. Effect of Diesel Soot Contaminated Oil on Engine Wear-Investigation of Novel Oil Formulations. *Tribol. Int.* **1999**, *32*, 687–699. [CrossRef]
38. Cusano, C.; Sliney, H.E. Dynamics of Solid Dispersions in Oil During the Lubrication of Point Contacts, Part I-Graphite NASA I. In Proceedings of the Annual Meeting of the American Society of Lubrication Engineers, Pittsburgh, PA, USA, 11–14 May 1981.
39. Rounds, F.G. Carbon: Cause of Diesel Engine Wear? *SAE Trans.* **1977**, *86*, 2870–2881.
40. Salehi, F.M.; Morina, A.; Neville, A. The Effect of Soot and Diesel Contamination on Wear and Friction of Engine Oil Pump. *Tribol. Int.* **2017**, *115*, 285–296. [CrossRef]
41. Salehi, F.M.; Khaemba, D.N.; Morina, A.; Neville, A. Corrosive–Abrasive Wear Induced by Soot in Boundary Lubrication Regime. *Tribol. Lett.* **2016**, *63*, 19. [CrossRef]
42. Olomolehin, Y.; Kapadia, R.; Spikes, H. Antagonistic Interaction of Antiwear Additives and Carbon Black. *Tribol. Lett.* **2010**, *37*, 49–58. [CrossRef]
43. *ASTM E2412*; Standard Practice for Condition Monitoring of Used Lubricants by Trend Analysis Using Fourier Transform Infrared (FT-IR) Spectrometry. ASTM International: Washington, DC, USA, 2018.
44. *DIN 51453*; Testing of Lubricants—Determination of Oxidation and Nitration of Used Motor Oils—Infrared Spectrometric Method. DIN (Deutsches Institut für Normung): Berlin, Germany, 2004.
45. *ASTM D664*; Standard Test Method for Acid Number of Petroleum Products by Potentiometric Titration. ASTM International: Washington, DC, USA, 2024.
46. *ISO 3771*; Petroleum Products—Determination of Base Number—Perchloric Acid Potentiometric Titration Method. International Organization for Standardization: Geneva, Switzerland, 2011.
47. Agocs, A.; Nagy, A.L.; Ristic, A.; Tabakov, Z.M.; Raffai, P.; Besser, C.; Frauscher, M. Oil Degradation Patterns in Diesel and Petrol Engines Observed in the Field—An Approach Applying Mass Spectrometry. *Lubricants* **2023**, *11*, 404. [CrossRef]
48. *ASTM D7042*; Standard Test Method for Dynamic Viscosity and Density of Liquids by Stabinger Viscometer (and the Calculation of Kinematic Viscosity). ASTM International: Washington, DC, USA, 2021.
49. Hakeem, M.; Anderson, J.; Surnilla, G.; Yamada, S.S. Characterization and Speciation of Fuel Oil Dilution in Gasoline Direct Injection (DI) Engines. In *Proceedings of the ASME 2015 Internal Combustion Engine Division Fall Technical Conference*; Volume 1: Large Bore Engines; Fuels; Advanced Combustion; American Society of Mechanical Engineers: New York, NY, USA, 2015.
50. *DIN 51777-2*; Testing of Mineral Oil Hydrocarbons and Solvents; Determination of Water Content According to Karl Fischer; Indirect Method. Deutsches Institut für Normung: Berlin, Germany, 1974.
51. *DIN ISO 7120*; Petroleum Products and Lubricants—Petroleum Oils and Other Fluids—Determination of Rust-Preventing Characteristics in the Presence of Water. Deutsches Institut für Normung: Berlin, Germany, 2000.
52. Eralytics Eraspec Oil—The Professional FTIR for Lube Oil Analysis. Available online: https://eralytics.com/products/eraspec-oil/ (accessed on 20 June 2026).
53. *ASTM D5185*; Standard Test Method for Multielement Determination of Used and Unused Lubricating Oils and Base Oils by Inductively Coupled Plasma Atomic Emission Spectrometry (ICP-AES). ASTM International: Washington, DC, USA, 2026.
54. Agocs, A. Lubricant Degradation in Internal Combustion Engines and Correlation with Artificial Ageing. Master's Thesis, Vienna University of Technology, Vienna, Austria, 2026.
55. Scherge, M.; Pöhlmann, K.; Gervé, A. Wear Measurement Using Radionuclide-Technique (RNT). *Wear* **2003**, *254*, 801–817. [CrossRef]

56. Frauscher, M.; Agocs, A.; Wopelka, T.; Ristic, A.; Ronai, B.; Holub, F.; Payer, W. Improving Sustainability by Enhanced Engine Component Lifetime through Friction Modifier Additives in Fuels. *Fuel* **2024**, *358*, 130102. [CrossRef]
57. Han, W.; Mu, X.; Liu, Y.; Wang, X.; Li, W.; Bai, C.; Zhang, H. A Critical Review of On-Line Oil Wear Debris Particle Detection Sensors. *J. Mar. Sci. Eng.* **2023**, *11*, 2363. [CrossRef]
58. Chambers, K.W.; Arneson, M.C.; Waggoner, C.A. An On-Line Ferromagnetic Wear Debris Sensor for Machinery Condition Monitoring and Failure Detection. *Wear* **1988**, *128*, 325–337. [CrossRef]
59. Sun, J.; Wang, L.; Li, J.; Li, F.; Fang, Y. An On-Line Imaging Sensor Based on Magnetic Deposition and Flowing Dispersion for Wear Debris Feature Monitoring. *Mech. Syst. Signal Process.* **2024**, *212*, 111321. [CrossRef]
60. Li, J.; Liang, X.; Dai, P.; Zhang, Z.; Wu, D.; Yan, J. Wear Particle Properties of the High-Pressure Common Rail Fuel System in Diesel Engines. *Powder Technol.* **2026**, *475*, 122322. [CrossRef]
61. Ronai, B. Evaluation of Chemical and Tribometrical Data of Engine Oils by Selected Multivariate Statistics. Master's Thesis, Vienna University of Technology, Vienna, Austria, 2021.
62. Varmuza, K.; Filzmoser, P. *Introduction to Multivariate Statistical Analysis in Chemometrics*; CRC Press: Boca Raton, FL, USA, 2016; ISBN 9780429145049.
63. Nagy, A.L.; Agocs, A.; Ronai, B.; Raffai, P.; Rohde-Brandenburger, J.; Besser, C.; Dörr, N. Rapid Fleet Condition Analysis through Correlating Basic Vehicle Tracking Data with Engine Oil Ft-Ir Spectra. *Lubricants* **2021**, *9*, 114. [CrossRef]
64. Zhou, F.; Shen, J.; Li, X.; Yang, K.; Wang, L. An Optimal Preprocessing Method for Predicting the Acid Number of Lubricating Oil Based on PLSR and Infrared Spectroscopy. *Lubricants* **2025**, *13*, 355. [CrossRef]
65. Sejkorová, M.; Kučera, M.; Hurtová, I.; Voltr, O. Application of FTIR-ATR Spectrometry in Conjunction with Multivariate Regression Methods for Viscosity Prediction of Worn-Out Motor Oils. *Appl. Sci.* **2021**, *11*, 3842. [CrossRef]
66. Sejkorová, M.; Šarkan, B.; Veselík, P.; Hurtová, I. FTIR Spectrometry with PLS Regression for Rapid TBN Determination of Worn Mineral Engine Oils. *Energies* **2020**, *13*, 6438. [CrossRef]
67. Macián, V.; Tormos, B.; García-Barberá, A.; Balaguer, A. Application Assessment of UV–Vis and NIR Spectroscopy for the Quantification of Fuel Dilution Problems on Used Engine Oils. *Fuel* **2023**, *333*, 126350. [CrossRef]
68. Rahimi, M.; Pourramezan, M.-R.; Rohani, A. Modeling and Classifying the In-Operando Effects of Wear and Metal Contaminations of Lubricating Oil on Diesel Engine: A Machine Learning Approach. *Expert Syst. Appl.* **2022**, *203*, 117494. [CrossRef]
69. Agocs, A.; Budnyk, S.; Frauscher, M.; Ronai, B.; Besser, C.; Dörr, N. Comparing Oil Condition in Diesel and Gasoline Engines. *Ind. Lubr. Tribol.* **2020**, *72*, 1033–1039. [CrossRef]
70. Animashaun, L.A. Tribochemistry of Boron-Containing Lubricant Additives on Ferrous Surfaces for Improved Internal Combustion Engine Performance. Ph.D. Thesis, University of Leeds, Leeds, UK, 2017.
71. The European Automobile Manufacturers' Association (ACEA) New EU Car Sales by Power Source. Available online: https://www.acea.auto/figure/fuel-types-of-new-passenger-cars-in-eu/ (accessed on 26 September 2025).
72. The European Automobile Manufacturers' Association (ACEA) New Car Registrations: +0.8% in 2024; Battery-Electric 13.6% Market Share. Available online: https://www.acea.auto/pc-registrations/new-car-registrations-0-8-in-2024-battery-electric-13-6-market-share/ (accessed on 26 September 2025).
73. The European Automobile Manufacturers' Association (ACEA) New Car Registrations: −0.7% in July 2025 Year-to-Date; Battery-Electric 15.6% Market Share. Available online: https://www.acea.auto/pc-registrations/new-car-registrations-0-7-in-july-2025-year-to-date-battery-electric-15-6-market-share/ (accessed on 26 September 2025).
74. Pedregosa, F.; Varoquaux, G.; Gramfort, A.; Michel, V.; Thirion, B.; Grisel, O.; Blondel, M.; Prettenhofer, P.; Weiss, R.; Dubourg, V.; et al. Scikit-Learn: Machine Learning in Python. *J. Mach. Learn. Res.* **2011**, *12*, 2825–2830.